



# Co-tri MOF-impregnated Aquivion® composites as proton exchange membranes for fuel cell applications

Subir Paul<sup>1</sup> · Sang-June Choi<sup>1</sup> · Hee Jin Kim<sup>1</sup>

Received: 17 September 2020 / Revised: 19 January 2021 / Accepted: 21 January 2021 / Published online: 1 February 2021  
© The Author(s), under exclusive licence to Springer-Verlag GmbH, DE part of Springer Nature 2021

## Abstract

In polymeric proton exchange membranes, the impregnation of filler materials, such as metal–organic frameworks (MOFs), has attracted considerable attention. Aquivion® is a state-of-the-art membrane used in fuel cells and electrolysis applications because of its mechanical stability and elevated proton conductivity at high temperatures. By applying the theory of coordination networks with the incorporation of a high-proton-conductive Co-tri MOF,  $\{[(\text{Co}(\text{bpy})(\text{H}_2\text{O})_4](\text{Hbtc})\cdot(\text{H}_2\text{O})_{1.5})_n\}$ , the proton conductivity of Aquivion® is improved. Co-tri MOF/Aquivion® composite membranes are prepared in different weight percentages using the solution casting method and are tested within a fuel cell system. The 1-wt.% Co-tri MOF/Aquivion® blend membrane shows an improved cell performance and a 66% increase in proton conductivity compared with that of the pristine Aquivion® membrane. The effect of Co-tri MOF on the Aquivion® membrane's structural morphology and thermal properties is also investigated.

**Keywords** Proton exchange membrane · Polymer electrolytes · Proton conductivity · Fuel cells

## Introduction

A polymer electrolyte membrane fuel cell (PEMFC) is one of the most common types of fuel cells. It has attracted research interest as a potential, efficient, and alternative energy source rather than as a fossil fuel resource. PEMFC directly transforms chemical energy into electrical energy with high efficiency, high power density, and less emission of environmental contaminants [1, 2]. As a result, it acquires more focus for both stationary and mobile power applications [3]. PEMFC is identified as a significant solution to achieve the European Union's greenhouse gas emission reduction target of 80% by 2050 [4]. Owing to its advantages such as fast start-up time, simple instrument structure, high power density, low operating temperature, and zero emission, PEMFC can be used extensively as a green-electrochemical system [5, 6]. The proton exchange membrane (PEM) is the principal part of PEMFC that ensures the separation of the feed gas and electrons

between the cathode and anode, thus enabling the transmission of protons [7]. To complete the ultimate redox reaction, PEM has to act as an electrolyte [8]. Owing to its exceptional conductivity of protons, perfluorosulfonic acid (PFSA), such as Nafion® and Aquivion®, is the most popular ionomer for PEM. In fuel cell applications, thin PFSA membranes are usually introduced to minimize membrane ohmic losses or resistance.

The ionomer's proton conductivity is measured by taking the equivalent weight as the parameter. The fabrication of a stable dispersion of ionomers with low equivalent weight is challenging [9]. In addition, in both low- and high-temperature PEMFC applications, PFSA short-side-chain (SSC) membranes have received extensive attention for use in membrane electrolytes owing to their high electrochemical and chemical degradation tolerance and excellent conductivity of proton [10–12]. Aquivion® is an SSC perfluorosulfonic membrane that is primarily established by Solvay Solexis for fuel cell applications [13] and has been tested for PEM electrolysis to a lesser extent [14]. The E83-06A PFSA SSC membrane used in this study is chemically stabilized and demonstrates an equivalent weight of 790 g/eq. For a specified equal weight, this ionomer displays a better glass transition temperature (T<sub>g</sub>) and crystallinity than those displayed by long-chain polymers [13]. Moreover, the thermal stability of Aquivion®

✉ Hee Jin Kim  
zammanbo814@knu.ac.kr

<sup>1</sup> Department of Architectural, Civil, Environmental Engineering, Kyungpook National University, 80 Daehakro, Bukgu, Daegu 41566, Korea

(140–160 °C) is better than that of Nafion (125 °C) [9]. The PEMFC's proton conductivity is the membrane's leading electrochemical energy transfer property. The membrane's proton resistance is known to be the key indicator of the ohmic overpotential of cell performance. The general objectives of the membrane are the improvement of proton conductivity, reduction of fuel crossover, and the realization of mechanical and thermal stability with a minimum level of degradation. Thus, improving the membrane properties of PEMFCs is a significant research topic in electrochemistry.

Metal–organic frameworks (MOFs) are porous coordination polymers made of metal ions and organic linkers. Because of their highly ordered crystallinity, dynamic behavior, postsynthetic functionalization, and well-designed and tailorable pores [15], MOFs have made advances in different applications such as gas storage [16], heterogeneous catalysis [17], and selective separation [18, 19]. Research has shown that MOFs are promising proton-conducting candidates owing to their proton-conduction potential and decent mechanical and thermal stabilities [20]. MOFs can be used to build active proton transfer pathways via the formation of hydrogen-bonded networks in pores by the judicious selection of organic ligands and metal centers [21, 22]. In addition, abundant MOF sites can be modified with functional groups for proton conduction, endowing them with a considerable ability for improved proton conduction [20, 23]. The use of a proton-conducting MOF (PCMOF) ionomer composite has the potential to enhance the performance of the membrane for PEMFC applications [24]. Generally, PEMs consist of acidic groups that function like a proton carrier and a hydrogen-bonded network, thus creating a passageway to facilitate the transfer of protons [25, 26].

Our group has demonstrated an increase in the conductance of protons by the introduction of a MOF in Nafion® membrane [26, 27]. Meanwhile, Elahi et al. developed Co-tri MOF with a crystalline nanoporous structure  $\{[(\text{Co}(\text{bpy})(\text{H}_2\text{O})_4](\text{Hbtc})(\text{H}_2\text{O})_{1.5})_n\}$  [28]. The Co-tri MOF consists of an organic linker with typical  $[(\text{Co}(\text{bpy})(\text{H}_2\text{O})_4)]^{2+}$  chains (bpy = 4,4'-bipyridine), which are neutralized by templated polycarboxylate anions, namely, benzene tri carboxylate (btc). Such MOFs, with varying degrees of protonation and ion carrier concentration, have a prominent part in crystal packing and in the development of well-directed H-linked networks, making such polymers exhibit an efficient performance in proton conductivity.

In this analysis, the improvement of the proton conductivity and performance by adding Co-tri MOF crystals in an Aquivion® composite under different circumstances has been studied. To compare the chemical characteristics, water uptake (WU) and ion-exchange capacity (IEC) were measured. The high crystallinity, chemi-mechanical stability, elemental compositions, and thermal stability of the membrane were also characterized using X-ray diffraction (XRD), Fourier

transform infrared (FT–IR), X-ray photoelectron spectroscopy (XPS), and thermogravimetric analysis (TGA). Finally, a membrane electrode assembly (MEA) was also developed to investigate the performance and durability of fuel cells.

## Experimental sections

### Materials

A solution of Aquivion® (D83-06A, EW = 790, Sigma Aldrich) was utilized for the preparation of the electrode. For fuel cell operation, a carbon-supported Pt catalyst (FuelcellsEtc, 0.3 mg/cm<sup>2</sup>, 40 wt.% Pt on carbon black) was used. Cobalt (II) nitrate hexahydrate (97%) was obtained from Daejung Chemicals and Metals. 4,4'-Bipyridine (98%) and 1,3,5-Benzenetricarboxylic acid (98%) were purchased from Alfa Aesar. All the reagents were used without further purification. Distilled water was used throughout the synthesis process. Commercial gas diffusion electrodes of 0.3 mg cm<sup>-2</sup> (40%) Pt loading on Vulcan XC72 carbon (235 μm thickness) were used.

### Preparation of Co-tri MOF

Co-tri MOF was crystallized by the method reported by Elahi et al [28].

In the first step, 0.291 g of  $\text{Co}(\text{NO}_3)_2 \cdot 6\text{H}_2\text{O}$  (cobalt (II) nitrate hexahydrate, 1.00 mmol), 0.156 g of  $\text{C}_{10}\text{H}_8\text{N}_2$  (4,4'-Bipyridine, 1.00 mmol), and 0.210 g of  $\text{C}_6\text{H}_3(\text{CO}_2\text{H})_3$  (Benzene-1,3,5-tricarboxylic acid, 1.00 mmol) were added to 25 mL of water and stirred for 30 min at 40 °C. The precipitate was then collected through filtration and allowed to gradually evaporate at room temperature (RT) for 6 days to form orange needle-shaped crystals.

### Preparation of composite membrane

The composite membranes of Co-tri MOF/Aquivion® were prepared via solution casting process. First, 6.5 g of Aquivion® and different wt.% of Co-tri MOF were thoroughly mixed for 30 min at 25 °C using an ultrasonicator to achieve a homogeneous solution. The MOF-polymer solutions were introduced into a petri dish and then dried for 2 h for solvent evaporation in a vacuum oven at 70 °C. Before peeling off from the petri dish, the membrane temperature was allowed to drop to RT. Finally, to increase the mechanical strength and crystallinity, the membranes were again annealed at 100 °C and 150 °C for 30 and 20 min, respectively.

The composite membranes were immersed in  $\text{H}_2\text{O}_2$  for 1 h, 0.5 M  $\text{H}_2\text{SO}_4$  for 1h, and water for 1 h to attain the desired activation. The thickness of the prepared composite

membranes was measured to be  $150 \pm 10$   $\mu\text{m}$  using a digital micrometer.

### Preparation of MEAs

The MEA is regarded as the core component of a PEMFC that regulates the overall performance and durability of a fuel cell system [29, 30]. The MEA was assembled by first placing the membrane between the anode and cathode, which are commercial gas diffusion electrodes. The MEAs were placed in the fuel cell hardware, which has a serpentine flow field pattern after hot pressing. The fabricated MEA has an active area of  $5\text{ cm}^2$ .

### Characterization of composite membranes

The molecular structures and morphologies of the developed samples were assessed by powder XRD (XRD, Bruker D2 PHASER, Germany) and field-emission SEM (FE–SEM, Hitachi JSM-6701F, JEOL), respectively. Before SEM tests, all of the samples were coated with gold for 70 s in a sputtering device. The degree of crystallinity of the developed membranes was calculated using Eq. (1).

$$\text{Degree of crystallinity} = \frac{A_c}{A_c + A_a} \quad (1)$$

where  $A_a$  and  $A_c$  are the regions of the amorphous and crystalline peaks, respectively [31]. The Origin Pro 2016 software was utilized to separate and fit the peaks to calculate  $A_a$  and  $A_c$ .

The FT–IR spectrum in the wavenumber range of  $400\text{--}4000\text{ cm}^{-1}$  was determined using a PerKinElmer Spectrum GX & Autoimage machine.

The chemical composition of the Co-tri MOF, pristine Aquivion®, and 1-wt.% Co-tri MOF/Aquivion® membrane were measured using an XPS (ESCA 5800, ULVAC-PHI, Inc, Kanagawa, Japan) equipped with a monochromated Al  $K\alpha$  X-ray source at 200 W.

The TGA was carried out in a nitrogen atmosphere using the TGA-2050, TA Instruments. The temperature was amplified from RT to  $700\text{ }^\circ\text{C}$  with an increment of  $10\text{ }^\circ\text{C}/\text{min}$ .

The WU percentages were calculated using the variation in the weight of the membranes based on Eq. (2).

$$\text{WU (\%)} = \frac{W_{\text{wet}} - W_{\text{dry}}}{W_{\text{dry}}} \times 100 \quad (2)$$

where  $w_{\text{dry}}$  corresponds to the membranes' dry weights and  $w_{\text{wet}}$  are the membranes' wet weights. The wet weights of the membranes were measured after submerging them for 24 h in the water at  $80\text{ }^\circ\text{C}$ .

The IEC of the PEMs were calculated using a general acid–base titration technique. Briefly, to exchange the  $\text{H}^+$  ions, the

developed membranes were submerged in  $\text{NaCl}(\text{aq})$  (1.0 M) solution under constant stirring for 24 h. With the  $\text{NaOH}(\text{aq})$  (0.01 M) solution, the membranes were then titrated. The IEC was calculated based on Eq. (3).

$$\text{IEC (meq.g}^{-1}\text{)} = \frac{C_{\text{NaOH}} \times V_{\text{NaOH}} \times n}{w_{\text{dry}}} \quad (3)$$

where  $C_{\text{NaOH}}$  is the concentration (0.01 M) of the NaOH solution,  $V_{\text{NaOH}}$  is the volume of the NaOH solution that is needed for the titration,  $n$  is the NaCl solution amount used for immersion throughout the titration process, and  $w_{\text{dry}}$  denotes the weight of initial predried membrane.

The number of sulfonic acid site ( $\lambda$ ) used for comparing the various materials, in which the WU was changed into water molecules, is determined according to Eq. (4).

$$\lambda = \frac{10 \times \text{WU}}{\text{IEC} \times M_{\text{H}_2\text{O}}} \quad (4)$$

where  $M_{\text{H}_2\text{O}}$  is the water molar weight, which is 18 g/mol. This equation presupposes that only the  $\text{SO}_3\text{H}$  group is liable for the absorption of water.

The oxidative stability was confirmed by calculating the membranes' loss of weight in the Fenton test [4 ppm Iron (II) sulfate hexahydrate and 3%  $\text{H}_2\text{O}_2$ ]. Initially, in an aqueous Iron (II) sulfate heptahydrate (4 ppm, 45 mL) solution, the weighted membranes were immersed and heated up to  $75\text{ }^\circ\text{C}$  for 30 min. Finally, 5 mL of 3%  $\text{H}_2\text{O}_2$  is transferred to the solutions. The deterioration of PEMs was paused after an interval of 1h. They were then rinsed several times with deionized water and weighed again. Fenton's reagents were replaced every 3 h to maintain a constant concentration of  $\text{H}_2\text{O}_2$ .

The weight loss of the membranes was calculated using Eq. (5):

$$\text{Weight loss} = \frac{m_i - m_f}{m_i} \times 100\% \quad (5)$$

where  $m_i$  and  $m_f$  are the dry weights of the membranes in Fenton's solution in the pre- and post-treatment, respectively.

The proton conductivities of the pristine Aquivion® cast and Co-tri MOF/Aquivion® composite membranes were measured by alternating current impedance spectroscopy (VersaSTAT 3, Almethec). Signal amplitude with an impedance range of 0.1–1000 kHz was applied. Two probe impedance analyses were conducted on the cast Aquivion® and blend membranes having an equivalent thickness at RT and 100% RH to generate Nyquist plots. Using Eq. (6), the conductivity of proton was measured.

$$\sigma = \frac{h}{R \times S} \quad (6)$$

where  $\sigma$  is the in-plane proton conductivity ( $\text{S cm}^{-1}$ ),  $h$  is the thickness of the membrane (cm),  $R$  is the resistance ( $\Omega$ ) acquired from the experiment, and  $S$  is the cross-sectional area ( $\text{cm}^2$ ) through which the protons pass [32]. At approximately 1 day before the experiment, the blend membranes were immersed in deionized water at RT.

Current voltage (I–V) analysis is the most commonly adopted method for characterizing fuel cell efficiency. It delivers a quantitative assessment of both the fuel cell power density and the overpotential. The performance of the fuel cell was evaluated by the CNL Fuel Cell Test Station (CNL Energy Corp) using air as the oxidant and  $\text{H}_2$  as the fuel. A stoichiometric ratio of 1.5: 2.5 for  $\text{H}_2$  and air, respectively, was used in the test. The limiting current density of hydrogen oxidation was determined using a dynamic potential range of 0.4–0.9 V at a scanning rate of  $2 \text{ mV s}^{-1}$ . Under two different conditions, every single cell was tested at  $80^\circ\text{C}$  at 75% RH and  $80^\circ\text{C}$  at 100% RH. The saturated liquid-vapor at the regulated dew point was progressively provided through the gas inlet to control the RH of the fuel gases. Once the cell activates at a fixed point, polarization curves of rising current density against the open-circuit voltage (OCV) were reported.

In a single cell, the developed MEAs were first set for the durability study, and the cell was conditioned for 3.5 h before developing the polarization curve. Using a step-sweeping technique (chronoamperometric), the accelerated lifetime (ALT) experiment was carried out at a sweeping voltage range from OCV to 0.6 V. The experiment parameters were at  $60^\circ\text{C}$  and 100% RH. The current density was evaluated for 500 cycles (approximately 35 h). Afterward, 1 cycle of the ALT test was conducted with a repetitive period for 4.5 min at a sweeping voltage range of OCV–0.6 V [33]. The interval sweeping voltage (15 s in each step) was 0.05 V, and only the current at 0.6 V was recorded in this study.

## Results and discussion

### X-ray diffraction

The polymer membrane crystallinity is an essential attribute that stabilizes the membrane even at high temperatures and was characterized by performing XRD diffractions. The XRD patterns of the pristine Aquivion®, 1-wt.% Co-tri MOF/Aquivion® and Co-tri MOF are presented in Fig. 1. The sharp peaks of Co-tri MOF patterns demonstrate a high crystallinity, which is an essential indication of effective proton conductivity. A broad diffraction pattern appearing in the XRD profiles at  $2\theta = 12\text{--}22^\circ$  for both membranes indicates a crystalline scattering of the polyfluorocarbon chains. The degree of crystallinity for 1-wt.% Co-tri MOF/Aquivion® membrane level (75.5%) is higher than that of the Aquivion® membrane

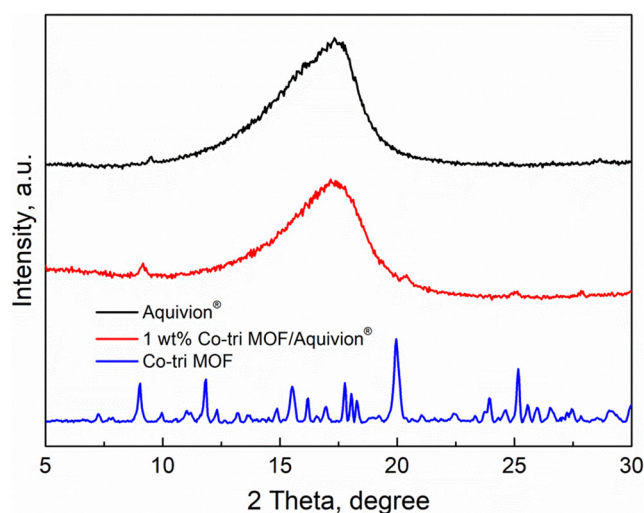


**Fig. 1** Powder X-ray diffraction (PXRD) patterns of cast Aquivion®, 1 wt.% Co-tri MOF/Aquivion® composite membranes, and Co-tri MOF

(74%) according to calculations of Eq. (1). The reasons for this improvement are apparently due to the thermal treatment (annealing) and the integration of crystalline Co-tri MOF. A clear peak shift at  $2\theta = 9^\circ$  and  $20^\circ$  toward the higher angle is observed in the 1-wt.% Co-tri MOF/Aquivion® compared to the Co-tri MOF. Peak shifting to a higher  $2\theta$  angle suggests a decreased interplanar spacing in the blended membrane with the introduction of the Co-tri MOF compared to that of the recast Aquivion®. According to the Bragg's equation ( $2d \sin\theta = n\lambda$ ) [34], the increase of  $\theta$  value is probably caused by the decrease of “d” owing to the fixed value of  $n\lambda$ .

### FT-IR spectroscopy

The FT-IR spectra of the pristine Aquivion® membrane, 1-wt.% Co-tri MOF/Aquivion® composite membrane, and Co-tri MOF in Fig. 2 show that there is a common Co-tri MOF

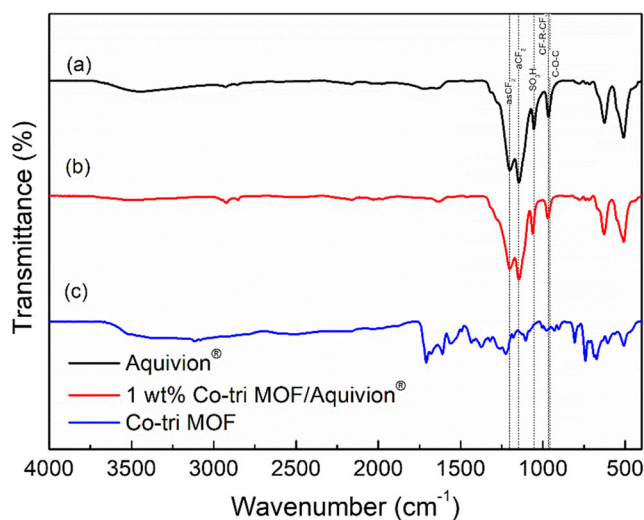


**Fig. 2** FTIR spectra of (a) Aquivion®, (b) 1 wt. % Co-tri MOF/Aquivion® composite membrane, and (c) pristine Co-tri MOF

hydrogen bond between the  $\text{SO}_4^{2-}$  anions and  $[\text{Co}(\text{bpy})(\text{H}_2\text{O})_4]^{2+}$  cations. The Co-tri FT-IR spectrum reveals that the peak characteristics attributable to the protonated  $-\text{COOH}$  group occurs at  $1719\text{ cm}^{-1}$  [28]. In the pristine Aquivion® and 1-wt.% Co-tri MOF/Aquivion® composite membrane, strong FT-IR absorption bands are first separated into the  $887.1\text{--}968.1\text{ cm}^{-1}$  C–O–C bands and the  $976.6\text{--}1010.6\text{ cm}^{-1}$  CF–R–CF<sub>3</sub> bands [35]. The typical sulfonic acid

group absorption of the perfluorosulfonic acid ionomer was then allocated approximately to the  $1014.4\text{--}1060.4\text{ cm}^{-1}$  bands. The absorption bands at  $1150.4\text{--}1161.6$  and  $1203.5\text{--}1360.7\text{ cm}^{-1}$  overlap the heavy symmetric and asymmetric stretching of the C–F. The peaks at  $2926\text{ cm}^{-1}$  are attributed to the  $\text{CH}_2\text{O}$  functional group [36, 37]. The FT-IR results indicate the successful grafting of the Co-tri MOF into the Aquivion®.

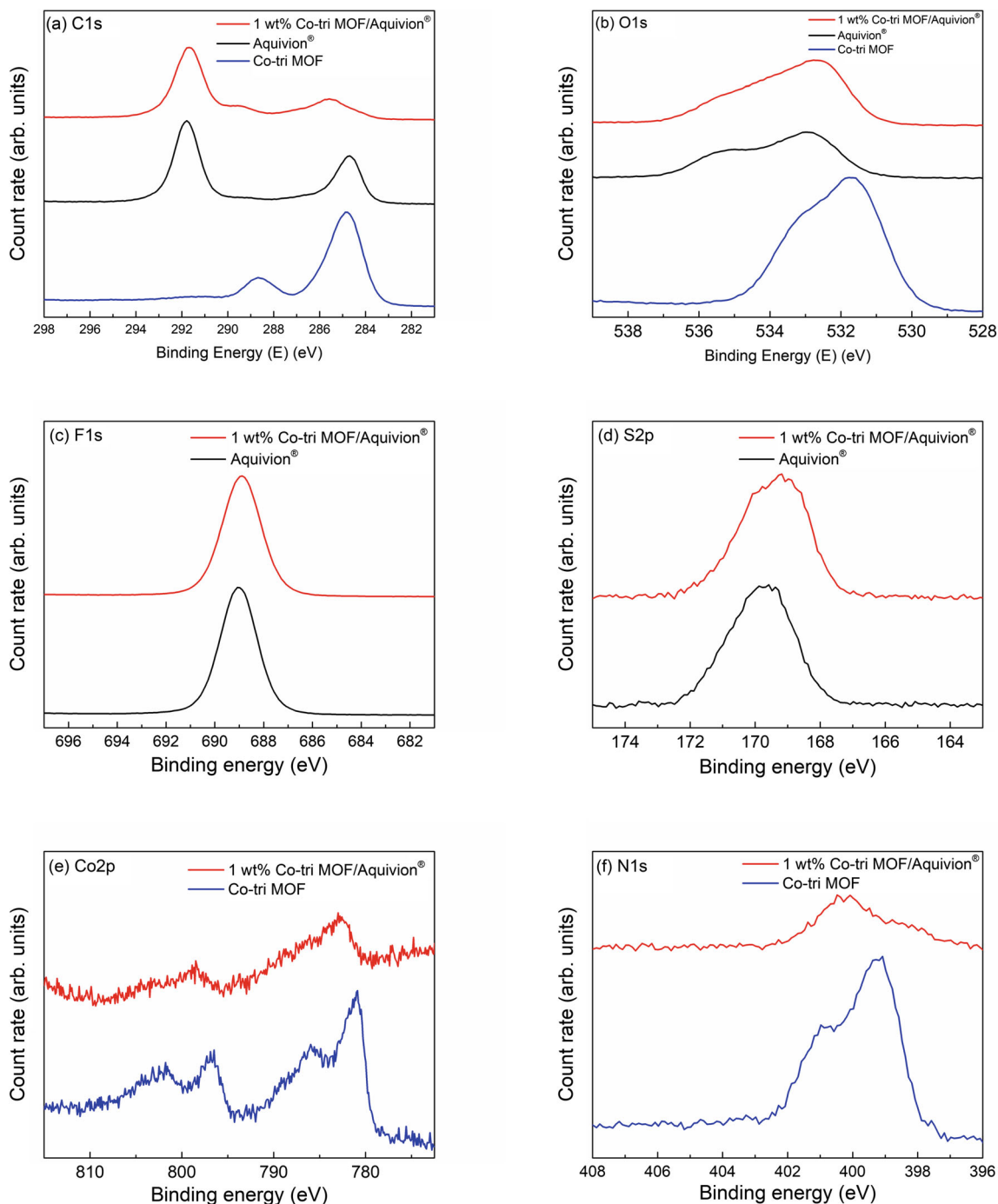


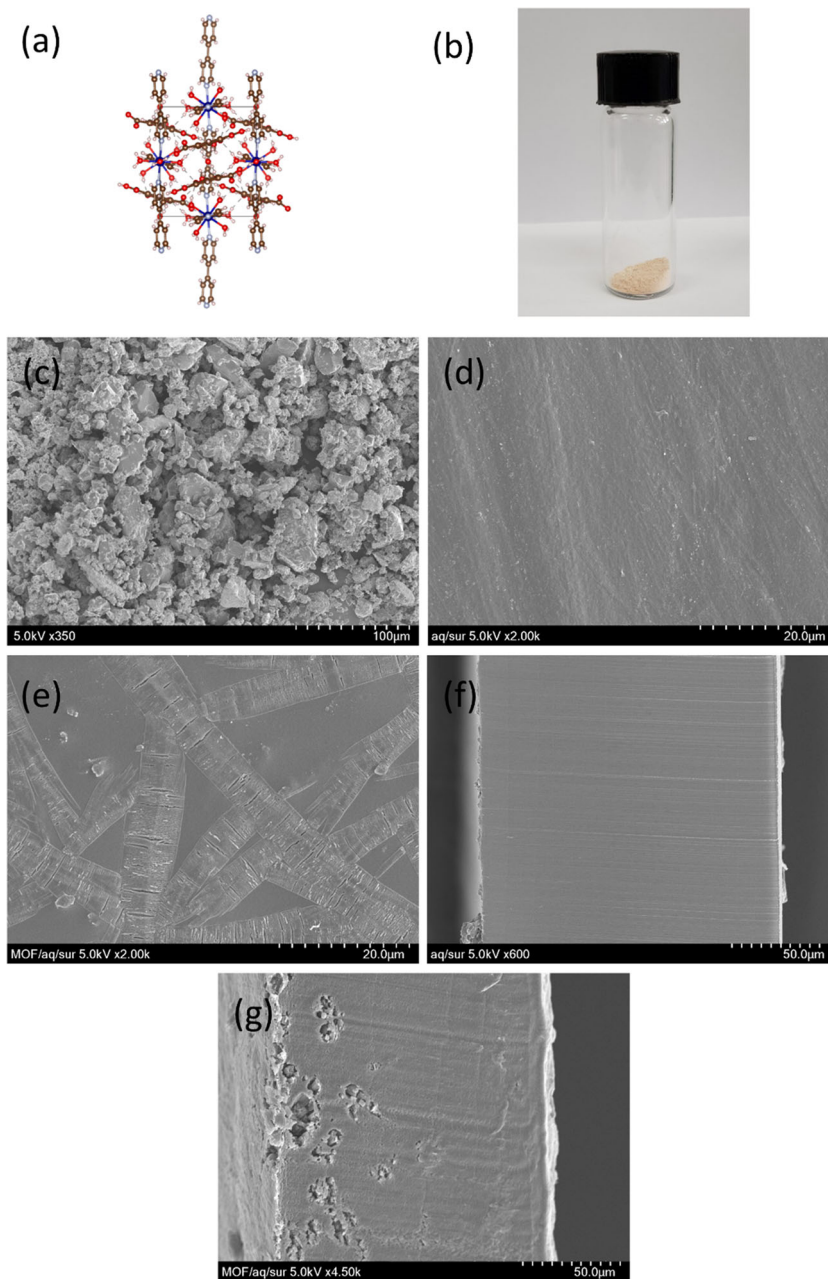
**Fig. 3** XPS spectra of Co-tri MOF, Pristine Aquivion®, and 1 wt.% Co-tri MOF/Aquivion® membrane. **a** C1s, **(b)** O1s, **(c)** F1s, **(d)** S2p, **(e)** Co2p, and **(f)** N1s core peaks

## XPS analyses

As shown in Fig. 3, the XPS spectra of Co-tri MOF, pristine Aquivion®, and 1-wt.% Co-tri MOF/Aquivion® membrane were measured at the C1s, O1s, F1s, S2p, Co2p, and N1s core levels. A binding energy  $E_b = 292.2$  eV is expected for carbon in the  $CF_2^-$  configuration for the pristine Aquivion® and 1-wt.% Co-tri MOF/Aquivion® membrane (Fig. 3a) [38]. The main C1s peak of the Co-tri MOF appears at 284.8 eV, which is identified as the  $sp^3$  carbon. For the 1-wt.% Co-tri MOF/Aquivion® membrane, the main peak position is downshifted by 0.6 eV. In the 1-wt.% Co-tri MOF/Aquivion®

membrane, a  $SO_3^-$  related peak appears near 533 eV (Fig. 3b). For the fluorine atoms, a binding energy of 689 eV is typically observed in the pristine Aquivion® and 1-wt.% Co-tri MOF/Aquivion® membrane (Fig. 3c) polymers [38]. Figure 3d shows the S2p spectrum for different membrane samples where sulfur of the sulfonic acid head group is assigned an  $E_b$  of  $\sim 170$  eV. The Co-tri MOF shows the primary cobalt and nitrogen atom signal at an  $E_b$  of 782 and 399 eV, respectively (Fig. 3e,f) [39]. A new signal is observed at 783 and 400 eV for 1-wt.% Co-tri MOF/Aquivion® membrane, corresponding to the primary cobalt and nitrogen atom, respectively. The C, O, Co, and N elements signals in the XPS

**Fig. 4** **(a)** Crystal structure of Co-tri MOF, **(b)** Co-tri MOF, FESEM images of **(c)** Co-tri MOF crystal, **(d)** surface of the pristine Aquivion®, **(e)** surface of 1 wt.% Co-tri MOF/Aquivion®, **(f)** cross sections of pristine Aquivion®, **(g)** cross sections of 1 wt.% Co-tri MOF/Aquivion®



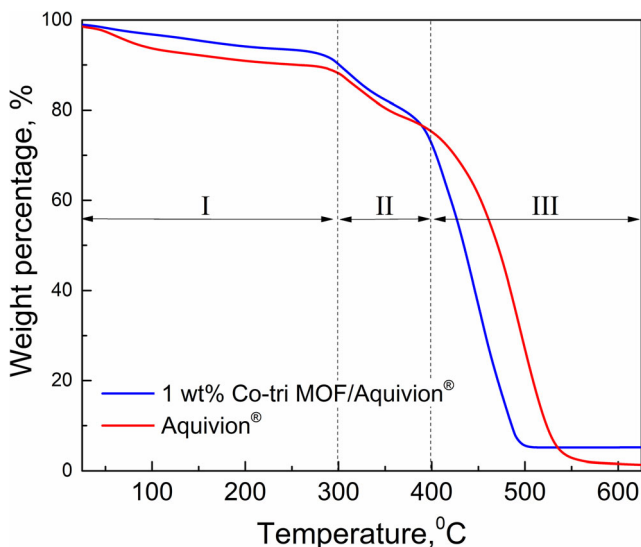


Fig. 5 Thermogram of the composite membranes (x-axis: 25 to 625 °C)

spectra of Co-tri MOF/Aquivion® membrane support the successful incorporation of Co-tri MOF into the Aquivion® membrane.

### FE-SEM based morphological study

Figure 4 presents the FE-SEM images of the Co-tri MOF and Co-tri MOF/Aquivion® composite membrane. The micrograph of the Co-tri MOF/Aquivion® composite membrane (Fig. 4e) confirms a well-compacted homogeneous microstructure. Owing to the excellent interfacial stability between the dispersion medium and the discontinuous phase, the Co-tri MOF crystals are incorporated well into the Aquivion® matrix, which can be helpful for the improvement of the conductivity of proton of the Co-tri MOF/Aquivion® blend membrane. Figure 4 also shows the cross sections of the pristine Aquivion® and 1-wt.% Co-tri MOF/Aquivion®.

### Thermal stability

The thermal stability and water retention data of Aquivion® and 1-wt.% Co-tri MOF/Aquivion® composite membrane was evaluated using the thermogravimetric (TG) curves displayed in Fig. 5.

Previous works reported that the whole weight loss of the membrane before reaching a temperature of 300 °C is

attributed to the removal of sulfonic acid groups and the evaporation of the physically and chemically absorbed water [40, 41]. On the other hand, the weight loss from 300 to 400 °C is due to the polymer side chain degradation. Beyond 400 °C, the weight loss is attributed to the thermal oxidation of the polymer membrane backbone [42]. The percentage weight loss data of Aquivion® and 1-wt.% Co-tri MOF /Aquivion® are presented in Table 1. Within 0–300 °C range, the 1-wt.% Co-tri MOF /Aquivion® displays lower water evaporation than Aquivion®. All the membranes are steady until 280 °C. After 280 °C, the stability begins to degrade due to the decomposition of the sulfonic acid group [43]. Besides the water content, the polymer backbone water retention is an indispensable part for the fuel cell process, specifically at elevated temperatures. Notably, the composite membrane shows high thermal membrane stability until 400 °C, suggesting that it fulfills the PEMFC’s operational criteria. However, the thermal stability of the composite membrane reduces after 400 °C due to the phase separation of the MOF crystals.

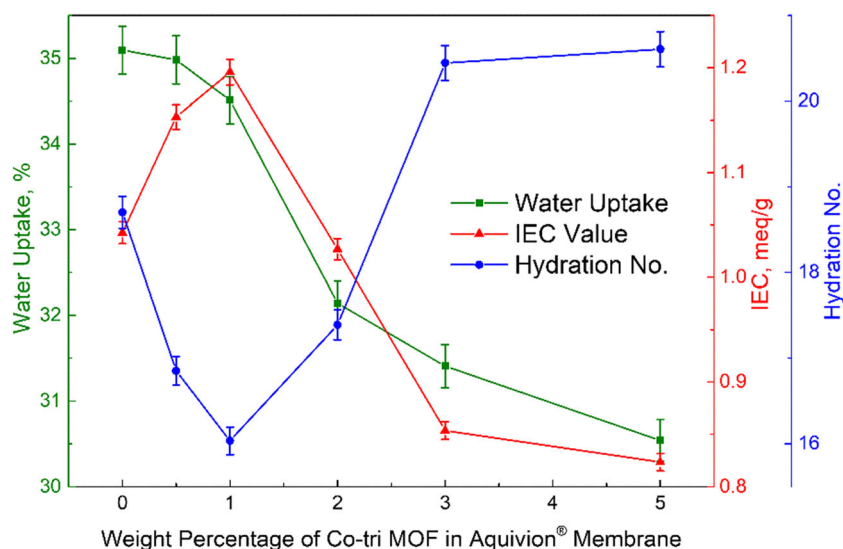
### WU, IEC, and hydration number

Typically, the WU or the hydration number  $\lambda$  is closely associated with the proton conductivity and the membrane mechanical properties [44]. The water molecule makes a significant contribution to the transfer of protons through the Grotthuss mechanism or the creation of hydrogen networks for Grotthuss mechanism [45]. A polymer membrane’s water absorption behavior influences its performance during operation at elevated temperatures. For example, excessive water absorption can cause dimensional deviations of a polymer membrane, which undermines its mechanical strength [46]. The integration of H<sub>2</sub>O molecules into the polymer membrane of Aquivion® substantially impacts the movement of protons, and the hydrated structures formed all over the sulfonate acid ions, which are negatively charged [47]. Co-tri MOF crystals decrease the number of hydrophilic SO<sub>3</sub><sup>-</sup> ions per volume unit of the Co-tri MOF/Aquivion® composite membrane. Hence, this Co-tri MOF/Aquivion® composite membrane shows a lower WU than the pristine Aquivion® cast membrane (Fig. 6). Alternatively, the spreading of Co-tri MOF in the Aquivion® Matrix may decrease the pores and lower the absorption efficiency of water molecules. Therefore, incorporating Co-tri MOF into the Aquivion® matrix will lower the

**Table 1** Summary of the weight-loss percentage in regions I, II, and III (Fig. 5) for pristine Aquivion® and the 1 wt.% Co-tri MOF/Aquivion® composite membrane

Membrane	Weight loss (%)		
	< 300 °C (I)	300–400 °C (II)	>400 °C (III)
Aquivion®	10.57	12.93	74.33
1 wt.% Co-tri MOF/Aquivion®	8.77	17.67	77.24

**Fig. 6** Water uptake, ion-exchange capacity, and hydration number of various weight percentages of Co-tri MOF/Aquivion® composite membranes



level of water absorption, which ultimately reduces swelling of the membrane and lowers the mechanical stress. As a result, increasing the Co-tri MOF content in the Aquivion® matrix lowers the rate of WU.

The IEC figures represent the number of acid-transferable groups within the membrane [48]. These groups are the hydrophilic components that regulate the ionic conductivity and WU [49]. Figure 6 represents the IEC data of the pristine Aquivion® membrane and that of the different wt.% Co-tri MOF/Aquivion® blend membranes. Under humidified conditions, the exchangeable Brønsted acidic sites of the Aquivion® matrix and the hydrophilic  $[\text{Co}(\text{bpy})(\text{H}_2\text{O})_4]^{2+}$  positively charged ions are embedded within the Co-tri MOF structure function as ion-exchange sites [50]. The proton carrier grows with the inclusion of Co-tri MOF, and a peak IEC value is observed at 1-wt.% Co-tri MOF/Aquivion®.

Further inclusion of the MOF above 1 wt.% reduces the IEC value. Another observed phenomenon is the reduction of the ratio of the sulfonic acid group to dimethyl ammonium cation with increased MOF content, which also leads to a reduced IEC value.

The hydration number ( $\lambda$ ) of various weight percentages of Co-tri MOF/Aquivion® composite membranes at RT is also shown in Fig. 6. From the WU results, it is evident that the 1-wt.% Co-tri MOF/Aquivion® blend membrane absorbs less water than the pristine Aquivion® membrane. Nevertheless, these membranes show higher  $\lambda$  values than other membranes owing to their higher IEC values. Such decreased hydration shows that the Co-tri MOF/Aquivion® blend membrane of 1 wt.% has better mechanical stability and resistivity to water compared to the other membranes.

### Oxidative stability

Figure 7 presents the findings of the chemical oxidative stability test conducted for 8 h. Throughout this experiment, free radicals were generated by the reaction of the iron source and hydrogen peroxide in an aqueous solution, as reported by Haber and Weiss [51, 52]. Various unstable intermediate species (free radicals) were formed that attacked the vulnerable portions of the membrane structure [51]. The membrane's weight loss percentage remained nearly constant during the first 1 h and progressively increased over time. Meanwhile, 1-wt.% Co-tri MOF/Aquivion® membrane showed the highest chemical stability compared with other membranes, with only 2.54% weight loss after 8 h. The incorporation of a minor quantity (such as 1 wt.% and 2 wt.%) of Co-tri MOF significantly enhanced the chemical stability of the Aquivion® membrane in a strong oxidative media [53], and the addition of more than 1 wt.% of MOF showed greater detriment of the weight of the membranes. This may be because the existence

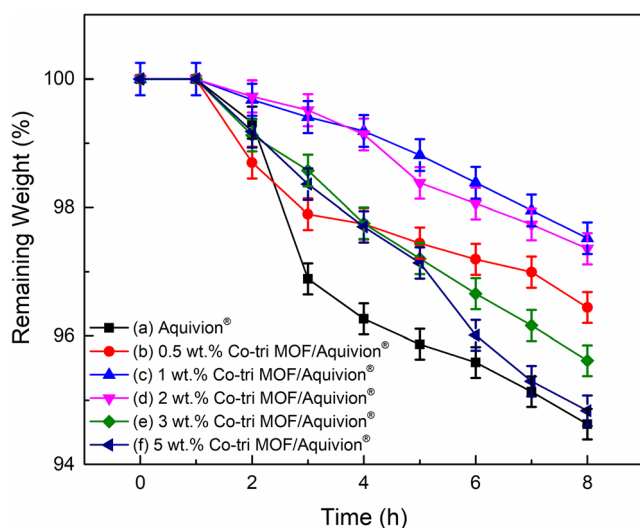
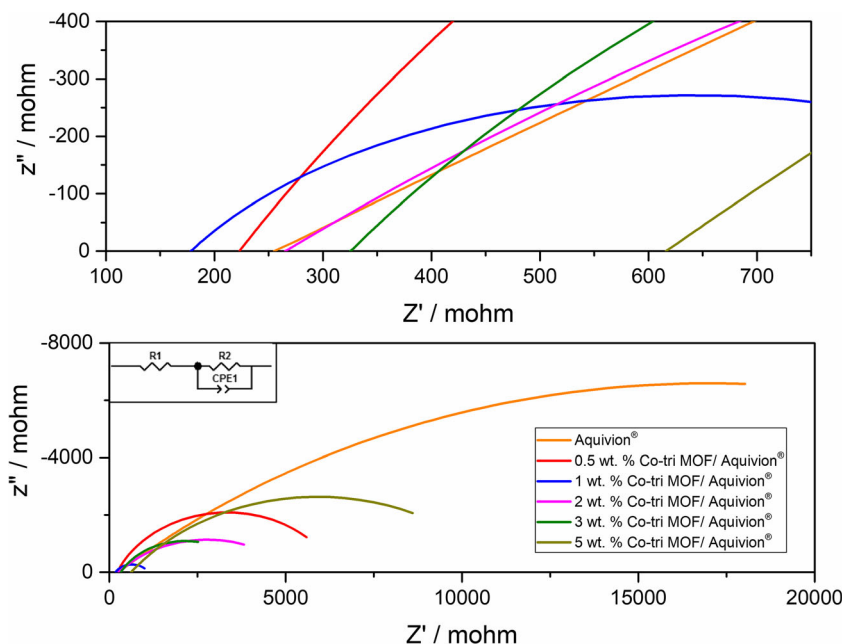


**Fig. 7** Fenton's reagent test of pristine Aquivion® and various weight percentages of Co-tri MOF/Aquivion® composite membranes



**Fig. 8** Nyquist impedance plots of various weight percentages of Co-tri MOF/Aquivion® composite membranes with the equivalent circuit (inset, bottom panel); in the circuit CPE, constant phase element, and R, resistance



of an additional filler is likely to result in the creation of certain particle agglomeration throughout the membrane matrix, which ultimately decreases the influence of MOF on the degradation agent [53]. Moreover, excess MOF weakens the polymer matrix surface compactness, making it easier for the molecule chain to be attacked by the HOO· or HO· of the Fenton reagent [54]. Such findings suggest that the addition of a minor quantity of Co-tri MOF considerably improves the chemical stability of the Aquivion® membrane.

**Conductivity measurement**

Proton conductivity is an integral variable to determine the PEM’s efficient transmission. A high proton conductivity results in a high power density via the electrolytic membrane [55]. Measurements were carried out using electrochemical impedance spectroscopy at RT and 100% RH. In this scenario, the equivalent circuit for the polymeric membranes such as Aquivion® or modified Aquivion® involves a free resistor and a resistor–capacitor circuit to measure the polymer’s bulk and interfacial properties. The ac impedance parameter

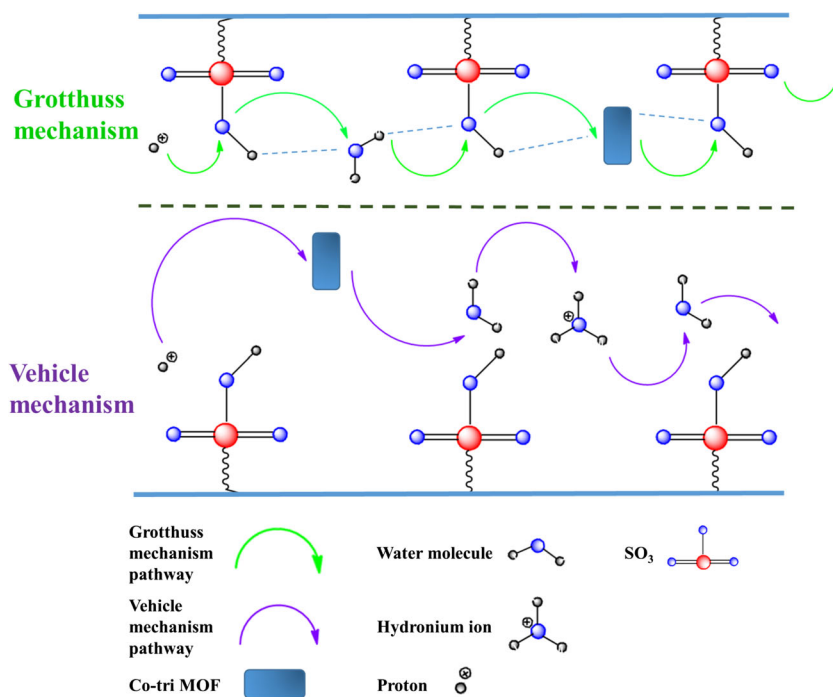
changes in the Nyquist diagrams were measured using the nonlinear and least-square fitting techniques of the Zview software.

Upon fitting with the corresponding circuit, the Nyquist plots of the membranes are achieved and displayed in Fig. 8. The graph shows that the incorporation of Co-tri MOF nanoparticles in the membrane matrix increases the conductivity of proton. Within a composite membrane, the proton conductivity relies on multiple factors including the spreading of the membrane inorganic filler, the membrane water absorption, the structural composition of the membrane, and the degree of interaction among the host polymer and the inorganic particles [56]. The 1-wt.% Co-tri MOF/Aquivion® blend membrane shows the least semicircle loop of the impedance response compared to all other membranes. The x-axis intercepts specify the ohmic resistance. The fitted resistance and proton conductivities in Table 2 clearly indicate that the conductivity of proton is improved primarily by MOF inclusion. The maximum conductivity ( $5.06 \times 10^{-2} \text{ S cm}^{-1}$ ) is observed for the 1-wt.% Co-tri MOF/Aquivion® blend membrane, which is 66% higher than that of the pristine Aquivion®

**Table 2** Fitted resistance and proton (H<sup>+</sup>) conductivity data for various weight percentages of Co-tri MOF/Aquivion® composite membranes

Membrane	Fitted resistance (ohm) <i>R</i>	H <sup>+</sup> conductivity (S cm <sup>-1</sup> ) $\sigma = L / (R \times A)$
Cast Aquivion®	0.255	0.0304
0.5 wt.% Co-tri MOF/Aquivion®	0.223	0.0404
1 wt.% Co-tri MOF/Aquivion®	0.178	0.0506
2 wt.% Co-tri MOF/Aquivion®	0.265	0.0340
3 wt.% Co-tri MOF/Aquivion®	0.325	0.0277
5 wt.% Co-tri MOF/Aquivion®	0.616	0.0146

**Fig. 9** The possible proton transfer mechanism in the Co-tri MOF/Aquivion® composite membrane



membrane. These data also correlate with the WU and IEC values of the membrane. In comparison with the earlier figures, the 1-wt.% Co-tri MOF/Aquivion® blend membrane shows a tremendous increase in proton conductivity, which is almost 3.5 times greater than that of the Nafion® membrane ( $1.1 \times 10^{-2} \text{ S cm}^{-1}$ ) [26].

The proton conductivity first increases with the inclusion of MOF, which agrees with the IEC and WU results. Similarly, the conductivity decreases owing to the decrease in SO<sub>3</sub>H groups per unit volume of each domain, which is a consequence of adding more than 1-wt.% MOF. This effect is also logically attributed to the lower WU in the composite membrane, which would contribute to a decreased number of

proton carriers. The Co-tri MOF shows a high proton conductivity of  $1.49 \times 10^{-1} \text{ S cm}^{-1}$  at 80 °C (98% RH) and a reasonable proton conductivity of  $2.92 \times 10^{-2} \text{ S cm}^{-1}$  at 40 °C (98% RH). In this study, the 1-wt.% Co-tri MOF/Aquivion® blend membrane is among the elevated proton-conducting membranes in situations with high moisture.

Two subsequent methods are liable for the transmission of protons in aqueous conditions: (i) the Grotthuss or hopping mechanism for the lower activation energy, wherein protons migrate from one transfer site to the neighboring site via hydrogen bonds (0–0.4 eV), and (ii) the vehicle mechanism for high activation energy, in which protons diffuse in the form of hydration, including H<sub>3</sub>O<sup>+</sup>, H<sub>5</sub>O<sub>2</sub><sup>+</sup>, and H<sub>9</sub>O<sub>4</sub><sup>+</sup> (>0.4 eV) (Fig.

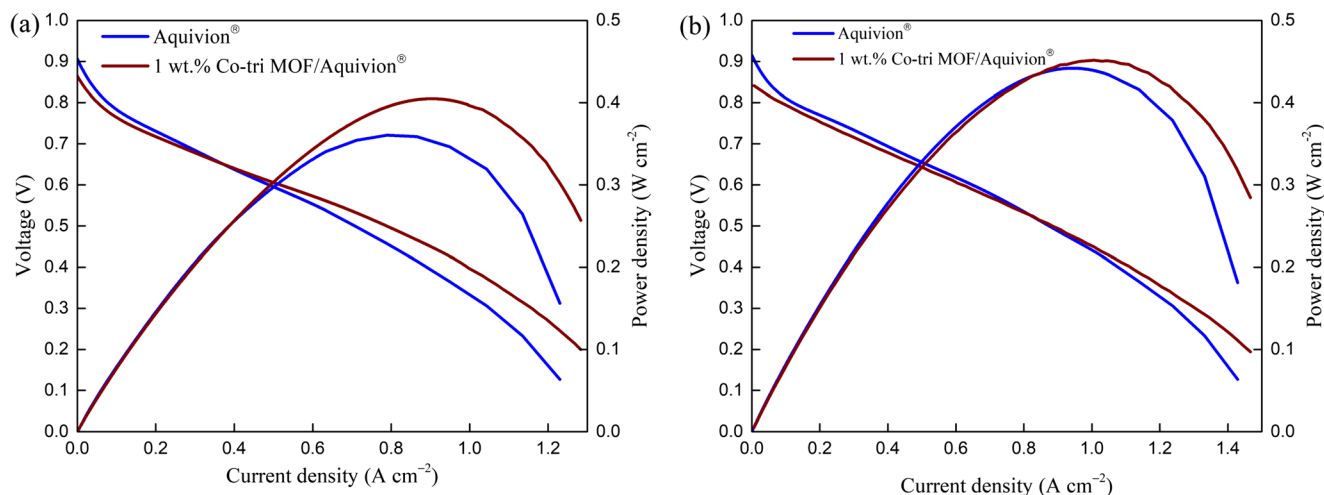


**Fig. 10** Fuel cell I–V curve of pristine Aquivion® and 1 wt.% Co-tri MOF/Aquivion® composite membranes under two different conditions: (a) 80 °C and 75% RH, (b) 80 °C and 100% RH

**Table 3** Power density characteristics for pristine Aquivion® and 1 wt.% Co-tri MOF/Aquivion® composite membranes under different conditions

Membrane	Temperature (°C)	RH (%)	Peak power density (W cm <sup>-2</sup> )	Current density at 0.6 V (A cm <sup>-2</sup> )
Aquivion®	80	100	0.442	0.647
Aquivion®	80	75	0.360	0.487
1 wt.% Co-tri MOF/Aquivion®	80	100	0.451	0.628
1 wt.% Co-tri MOF/Aquivion®	80	75	0.405	0.517

9) [57]. The Co-tri MOF lattice water acts as a mediator between the neighboring carboxylic group under humidified conditions. The carriers with a high symmetric configuration (Co-tri orthorhombic system) as well as Co-tri protons reliably and isotopically contribute to the superprotonic conductivity of the membrane [58]. According to the above technique, the continuous formation and breakage of hydrogen bonds along the proton transfer path, which is dispersed through the Co-tri MOF and the Aquivion® matrices, facilitate the increase of PC.

**Performance test in single cell**

The fuel cell performances of the pristine Aquivion® membrane and 1-wt.% Co-tri MOF/Aquivion® membrane in two separate circumstances are presented in Fig. 10. Obviously, the addition of Co-tri MOF will improve the power density as predicted based on the data in Fig. 8. At 80 °C and 100% RH, the cell performance is notably greater for the Co-tri MOF/Aquivion® blend membrane compared to the pristine Aquivion® membrane. At 0.6 V, the current density reaches 0.628 A cm<sup>-2</sup> for the Co-tri MOF/Aquivion® membrane. The current density improves from 0.487 A cm<sup>-2</sup> for the pristine

Aquivion® membrane to 0.517 A cm<sup>-2</sup> for the Co-tri MOF/Aquivion® blend membrane at 80 °C and 75% RH. Predictably, the improved performance of the Co-tri MOF/Aquivion® blend membrane is due to the improved proton conductivity and optimized water retention capacity of the membrane. A high power density of 0.451 W cm<sup>-2</sup> is witnessed for the Co-tri MOF/Aquivion® blend membrane at 80 °C and 100% RH, while 0.442 W cm<sup>-2</sup> is the peak power density of the pristine Aquivion® membrane. Table 3 summarizes the power density features of the Aquivion® and 1-wt.% Co-tri MOF/Aquivion® blend membranes in dissimilar circumstances.

**Durability test**

Figure 11 shows the ALT test outcomes of the Aquivion® and 1% wt. Co-tri MOF/Aquivion® blend membranes. The Co-tri MOF/Aquivion® blend membrane current density reduction rate is 3.46 mA cm<sup>-2</sup>, which is lower than that of the pristine Aquivion® membrane (3.63 mA cm<sup>-2</sup>). The data shows that the results are in good agreement with the oxidative stability test. The thermally and mechanically stable Co-tri MOF component in the Aquivion®, which can result in a superior proton conductivity, may be the reason for the improved cell durability of the 1-wt.% Co-tri MOF/Aquivion® blend membrane than the pristine Aquivion® membrane [33].

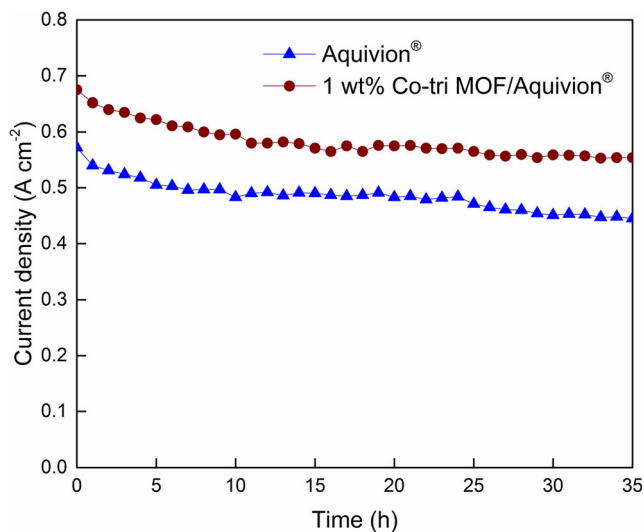


**Fig. 11** ALT test at 0.6 V of pristine Aquivion® and 1 wt.% Co-tri MOF/Aquivion® membranes under 60 °C and 100% RH

**Conclusions**

In summary, a novel Co-tri MOF/Aquivion® blend membrane utilizing an SSC Aquivion® PFSA is established in this study. The structures and properties of the Co-tri MOF/Aquivion® composite membranes are also studied. The physical characterization results of SEM, FT-IR, and XRD indicate that the Co-tri MOF was dispersed homogeneously in the Aquivion® polymer matrix. The TGA results show that the polymer electrolyte membranes are thermally stable up to ~280 °C. The 1-wt.% Co-tri MOF/Aquivion® blend membrane shows an enhanced proton conductivity of 5.06 × 10<sup>-2</sup> S cm<sup>-1</sup> at RT and 100% RH compared to the pristine Aquivion® membrane. The single-cell performance test reveals

that the 1-wt.% Co-tri MOF/Aquivion® blend membrane gives a better performance than the pristine Aquivion® membrane. The Co-tri MOF/Aquivion® blend demonstrates an outstanding physical stability in addition to enhanced proton conductivity and a decent single-cell performance. According to these findings, the Co-tri MOF/Aquivion® composite membrane is an excellent potential candidate for the design of a robust polymer membrane composite for electrochemical applications.

**Funding** This research was supported by the Ministry of Education which is funded by the Brain Korea 21 Plus (21A20132000001).

## References

- Raja K, Raja Pugalanthi M, Ramesh Prabhu M (2019) Investigation on SPEEK/PAI/SrTiO<sub>3</sub>-based nanocomposite membrane for high-temperature proton exchange membrane fuel cells. *Ionics (Kiel)* 25: 5177–5188. <https://doi.org/10.1007/s11581-019-03100-7>
- Talukdar K, Ripan MA, Jahnke T et al (2020) Experimental and numerical study on catalyst layer of polymer electrolyte membrane fuel cell prepared with diverse drying methods. *J Power Sources* 461:228169. <https://doi.org/10.1016/j.jpowsour.2020.228169>
- Imran MA, He G, Wu X et al (2019) Fabrication and characterization of sulfonated polybenzimidazole/sulfonated imidized graphene oxide hybrid membranes for high temperature proton exchange membrane fuel cells. *J Appl Polym Sci* 136:1–13. <https://doi.org/10.1002/app.47892>
- Talukdar K, Helmlly S, Schulze M et al (2019) Enveloping of catalyst powder by ionomer for dry spray coating in polymer electrolyte membrane fuel cells. *J Power Sources* 424:82–90. <https://doi.org/10.1016/j.jpowsour.2019.03.093>
- He G, Chang C, Xu M et al (2015) Tunable nanochannels along graphene oxide/polymer core-shell nanosheets to enhance proton conductivity. *Adv Funct Mater* 25:7502–7511. <https://doi.org/10.1002/adfm.201503229>
- Maiti J, Kakati N, Lee SH et al (2012) Where do poly(vinyl alcohol) based membranes stand in relation to Nafion® for direct methanol fuel cell applications? *J Power Sources* 216:48–66. <https://doi.org/10.1016/j.jpowsour.2012.05.057>
- Sahin A, Tasdemir HM, Ar İ (2019) Improved performance and durability of sulfonated polyether ether ketone/cerium phosphate composite membrane for proton exchange membrane fuel cells. *Ionics (Kiel)* 25:5163–5175. <https://doi.org/10.1007/s11581-019-03109-y>
- Wong CY, Wong WY, Ramya K et al (2019) Additives in proton exchange membranes for low- and high-temperature fuel cell applications: a review. *Int J Hydrog Energy* 44:6116–6135. <https://doi.org/10.1016/j.ijhydene.2019.01.084>
- Talukdar K, Gazdzicki P, Friedrich KA (2019) Comparative investigation into the performance and durability of long and short side chain ionomers in polymer electrolyte membrane fuel cells. *J Power Sources* 439:227078. <https://doi.org/10.1016/j.jpowsour.2019.227078>
- Paul S, Choi S-J, Kim HJ (2020) Enhanced proton conductivity of a Zn (II)-based MOF/Aquivion composite membrane for PEMFC applications. *Energy Fuel* 34:10067–10077
- Li X, Li Z, Yang J (2014) Proposed photosynthesis method for producing hydrogen from dissociated water molecules using incident near-infrared light. *Phys Rev Lett* 112:1–5. <https://doi.org/10.1103/PhysRevLett.112.018301>
- Zhao N, Edwards D, Lei C et al (2013) The importance of water transport on short-side chain perfluorosulfonic acid membrane fuel cells operating under low relative humidity. *J Power Sources* 242: 877–883. <https://doi.org/10.1016/j.jpowsour.2013.05.176>
- Stassi A, Gatto I, Passalacqua E et al (2011) Performance comparison of long and short-side chain perfluorosulfonic membranes for high temperature polymer electrolyte membrane fuel cell operation. *J Power Sources* 196:8925–8930. <https://doi.org/10.1016/j.jpowsour.2010.12.084>
- Wu X, Scott K, Puthiyapura V (2012) Polymer electrolyte membrane water electrolyser with Aquivion® short side chain perfluorosulfonic acid ionomer binder in catalyst layers. *Int J Hydrog Energy* 37:13243–13248. <https://doi.org/10.1016/j.ijhydene.2012.06.093>
- Shalini S, Dhavale VM, Eldho KM et al (2016) 1000-Fold enhancement in proton conductivity of a MOF using post-synthetically anchored proton transporters. *Sci Rep* 6:1–8. <https://doi.org/10.1038/srep32489>
- Stavila V, Bhakta RK, Alam TM et al (2012) Reversible hydrogen storage by NaAlH<sub>4</sub> confined within a titanium-functionalized MOF-74(Mg) nanoreactor. *ACS Nano* 6:9807–9817. <https://doi.org/10.1021/nm304514c>
- Jiang D, Mallat T, Krumeich F, Baiker A (2008) Copper-based metal-organic framework for the facile ring-opening of epoxides. *J Catal* 257:390–395. <https://doi.org/10.1016/j.jcat.2008.05.021>
- Wang C, Liu D, Lin W (2013) Metal-organic frameworks as a tunable platform for designing functional molecular materials. *J Am Chem Soc* 135:13222–13234. <https://doi.org/10.1021/ja308229p>
- Ye S, Jiang X, Ruan LW et al (2013) Post-combustion CO<sub>2</sub> capture with the HKUST-1 and MIL-101(Cr) metal-organic frameworks: adsorption, separation and regeneration investigations. *Microporous Mesoporous Mater* 179:191–197. <https://doi.org/10.1016/j.micromeso.2013.06.007>
- Shimizu GKH, Taylor JM, Kim SR (2013) Proton conduction with metal-organic frameworks. *Science* 341(80):354–355. <https://doi.org/10.1126/science.1239872>
- Sadakiyo M, Okawa H, Shigematsu A et al (2012) Promotion of low-humidity proton conduction by controlling hydrophilicity in layered metal-organic frameworks. *J Am Chem Soc* 134:5472–5475. <https://doi.org/10.1021/ja300122r>
- Jeong NC, Samanta B, Lee CY et al (2012) Coordination-chemistry control of proton conductivity in the iconic metal-organic framework material HKUST-1. *J Am Chem Soc* 134:51–54. <https://doi.org/10.1021/ja2110152>
- Ponomareva VG, Kovalenko KA, Chupakhin AP et al (2012) Imparting high proton conductivity to a metal-organic framework material by controlled acid impregnation. *J Am Chem Soc* 134: 15640–15643. <https://doi.org/10.1021/ja305587n>
- Sun H, Tang B, Wu P (2017) Two-dimensional zeolitic imidazolate framework/carbon nanotube hybrid networks modified proton exchange membranes for improving transport properties. *ACS Appl Mater Interfaces* 9:35075–35085. <https://doi.org/10.1021/acsami.7b13013>
- Firouz Tadavani K, Abdolmaleki A, Molavian MR et al (2017) Synergistic behavior of phosphonated and sulfonated groups on proton conductivity and their performance for high-temperature proton exchange membrane fuel cells (PEMFCs). *Energy Fuel* 31: 11460–11470. <https://doi.org/10.1021/acs.energyfuels.7b01065>

26. Kabir MDL, Kim HJ, Choi S-J (2018) Highly proton conductive Zn(II)-based metal-organic framework/Nafion® composite membrane for fuel cell application. *Sci Adv Mater* 10:1630–1635. <https://doi.org/10.1166/sam.2018.3355>
27. Kim HJ, Talukdar K, Choi SJ (2016) Tuning of Nafion® by HKUST-1 as coordination network to enhance proton conductivity for fuel cell applications. *J Nanopart Res* 18:47. <https://doi.org/10.1007/s11051-016-3346-9>
28. Elahi SM, Chand S, Deng WH et al (2018) Polycarboxylate-templated coordination polymers: role of templates for superprotonic conductivities of up to 10<sup>-1</sup> S cm<sup>-1</sup>. *Angew Chem* 57:6662–6666. <https://doi.org/10.1002/anie.201802632>
29. Talukdar K, Delgado S, Lagarteira T et al (2019) Minimizing mass-transport loss in proton exchange membrane fuel cell by freeze-drying of cathode catalyst layers. *J Power Sources* 427:309–317. <https://doi.org/10.1016/j.jpowsour.2019.04.094>
30. Martina P, Gayathri R, Pugalenthi MR et al (2020) Nanosulfonated silica incorporated SPEEK/SPVdF-HFP polymer blend membrane for PEM fuel cell application. *Ionics (Kiel)* 26:3447–3458. <https://doi.org/10.1007/s11581-020-03478-9>
31. Aziz SB, Abdullah OG, Rasheed MA, Ahmed HM (2017) Effect of high salt concentration (HSC) on structural, morphological, and electrical characteristics of chitosan based solid polymer electrolytes. *Polymers (Basel)* 9. <https://doi.org/10.3390/polym9060187>
32. Talukdar K, Kim HJ, Kim YH et al (2014) Polyacrylamide/Nafion® semi-interpenetrating networks as proton-conducting membrane of direct methanol fuel cell. *Sci Adv Mater* 6:2389–2394. <https://doi.org/10.1166/sam.2014.2190>
33. Lee C, Park J, Jeon Y et al (2017) Phosphate-modified TiO<sub>2</sub>/ZrO<sub>2</sub> nanofibrous web composite membrane for enhanced performance and durability of high-temperature proton exchange membrane fuel cells. *Energy Fuel* 31:7645–7652. <https://doi.org/10.1021/acs.energyfuels.7b00941>
34. Liu L, Li Z, Che Q (2019) Multilayered membrane electrolytes based on aramid nanofibers for high-temperature proton exchange membrane fuel cells. *ACS Appl Nano Mater* 2:2160–2168. <https://doi.org/10.1021/acsnm.9b00144>
35. Jeon Y, Hwang HK, Park J et al (2014) Temperature-dependent performance of the polymer electrolyte membrane fuel cell using short-side-chain perfluorosulfonic acid ionomer. *Int J Hydrog Energy* 39:11690–11699. <https://doi.org/10.1016/j.ijhydene.2014.05.105>
36. Liang Z, Chen W, Liu J et al (2004) FT-IR study of the microstructure of Nafion® membrane. *J Membr Sci* 233:39–44. <https://doi.org/10.1016/j.memsci.2003.12.008>
37. Xiao P, Li J, Tang H et al (2013) Physically stable and high performance Aquivion/ePTFE composite membrane for high temperature fuel cell application. *J Membr Sci* 442:65–71. <https://doi.org/10.1016/j.memsci.2013.04.014>
38. Friedman AK, Shi W, Losovyj Y et al (2018) Mapping microscale chemical heterogeneity in Nafion membranes with X-ray photoelectron spectroscopy. *J Electrochem Soc* 165:H733–H741. <https://doi.org/10.1149/2.0771811jes>
39. Geng H-Z, Kim KK, Lee YH (2008) Recent progress in carbon nanotube-based flexible transparent conducting film. *Carbon Nanotub Assoc Devices* 7037:70370A. <https://doi.org/10.1117/12.796143>
40. Tian SH, Shu D, Wang SJ et al (2007) Poly(arylene ether)s with sulfonic acid groups on the backbone and pendant for proton exchange membranes used in PEMFC applications. *Fuel Cells* 7:232–237. <https://doi.org/10.1002/fuce.200600005>
41. Mulmi S, Park CH, Kim HK et al (2009) Surfactant-assisted polymer electrolyte nanocomposite membranes for fuel cells. *J Membr Sci* 344:288–296. <https://doi.org/10.1016/j.memsci.2009.08.028>
42. Pan H, Chen S, Jin M et al (2018) Preparation and properties of sulfonated polybenzimidazole-polyimide block copolymers as electrolyte membranes. *Ionics (Kiel)* 24:1629–1638. <https://doi.org/10.1007/s11581-017-2341-1>
43. Talukdar, Krishan; Kim, Hee Jin; kim, Young HO; Park, Younjin; Lee, Ho-Chung; Choi SJ (2015) Proton-conducting membranes from Nafion/polystyrene sulfonate composite for fuel cell applications. *J Nanoelectron Optoelectron* 10:
44. Kreuer KD (2001) On the development of proton conducting polymer membranes for hydrogen and methanol fuel cells. *J Membr Sci* 185:29–39. [https://doi.org/10.1016/S0376-7388\(00\)00632-3](https://doi.org/10.1016/S0376-7388(00)00632-3)
45. Hu F, Li T, Zhong F, et al (2020) Preparation and properties of chitosan/acidified attapulgite composite proton exchange membranes for fuel cell applications. *J Appl Polym Sci* 1–9. <https://doi.org/10.1002/app.49079>
46. Ahmed S, Cai Y, Ali M et al (2019) Preparation and performance of nanoparticle-reinforced chitosan proton-exchange membranes for fuel-cell applications. *J Appl Polym Sci* 136:1–7. <https://doi.org/10.1002/app.46904>
47. Bose S, Kuila T, Nguyen TXH et al (2011) Polymer membranes for high temperature proton exchange membrane fuel cell: recent advances and challenges. *Prog Polym Sci* 36:813–843. <https://doi.org/10.1016/j.progpolymsci.2011.01.003>
48. Taghizadeh MT, Vatanparast M (2016) Ultrasonic-assisted synthesis of ZrO<sub>2</sub>nanoparticles and their application to improve the chemical stability of Nafion membrane in proton exchange membrane (PEM) fuel cells. *J Colloid Interface Sci* 483:1–10. <https://doi.org/10.1016/j.jcis.2016.08.014>
49. Guimet A, Chikh L, Morin A, Fichet O (2016) Strengthening of perfluorosulfonic acid ionomer with sulfonated hydrocarbon polyelectrolyte for application in medium-temperature fuel cell. *J Membr Sci* 514:358–365. <https://doi.org/10.1016/j.memsci.2016.04.031>
50. Talukdar K, Kim HJ, Kabir ML (2017) Reinforcing Nafion® with poly(ethylene-alt-maleic anhydride) as water-absorbing and film-forming polymer. *J Nanoelectron Optoelectron* 12:820–824. <https://doi.org/10.1166/jno.2017.2058>
51. Kinumoto T, Inaba M, Nakayama Y et al (2006) Durability of perfluorinated ionomer membrane against hydrogen peroxide. *J Power Sources* 158:1222–1228
52. Kabir L, Paul S, Choi S-J, Kim HJ (2020) Improved electrochemical and mechanical properties of poly(vinylpyrrolidone)/Nafion® membrane for fuel cell applications. *J Nanosci Nanotechnol* 20: 7793–7799
53. Parnian MJ, Rowshanzamir S, Alipour Moghaddam J (2018) Investigation of physicochemical and electrochemical properties of recast Nafion nanocomposite membranes using different loading of zirconia nanoparticles for proton exchange membrane fuel cell applications. *Mater Sci Energy Technol* 1:146–154. <https://doi.org/10.1016/j.mset.2018.06.008>
54. Ru C, Li Z, Zhao C et al (2018) Enhanced proton conductivity of sulfonated hybrid poly(arylene ether ketone) membranes by incorporating an amino-sulfo bifunctionalized metal-organic framework for direct methanol fuel cells. *ACS Appl Mater Interfaces* 10:7963–7973. <https://doi.org/10.1021/acsmi.7b17299>
55. Nakabayashi K, Higashihara T, Ueda M (2010) Polymer electrolyte membranes based on cross-linked highly sulfonated multiblock copoly(ether sulfone)s. *Macromolecules* 43:5756–5761. <https://doi.org/10.1021/ma100903v>

56. Devrim Y, Devrim H (2015) PEM fuel cell short stack performances of silica doped nanocomposite membranes. *Int J Hydrog Energy* 40:7870–7878. <https://doi.org/10.1016/j.ijhydene.2014.11.018>
57. Rao Z, Feng K, Tang B, Wu P (2017) Construction of well interconnected metal-organic framework structure for effectively promoting proton conductivity of proton exchange membrane. *J Membr Sci* 533:160–170. <https://doi.org/10.1016/j.memsci.2017.03.031>
58. Chen Y, Thorn M, Christensen S et al (2010) Enhancement of anhydrous proton transport by supramolecular nanochannels in comb polymers. *Nat Chem* 2:503

**Publisher's note** Springer Nature remains neutral with regard to jurisdictional claims in published maps and institutional affiliations.